RESEARCH PAPER
Contrib. Sci. & Tech Eng, 2025, 2(4)
Homepage: https://cste.journals.umz.ac.ir/
DOI:10.22080/cste.2025.28914.1026

Effect of Temperature on the Natural Frequency of Multi-Directional Functionally Graded Rectangular Plates on an Elastic Foundation using Three-Dimensional Elasticity Theory

Mahdi Adineh [1]*, Hossein Estiri [2]

[1] *Department of Mechanical Engineering, University of Gonabad, Gonabad, Iran.*

[2] *Department of Civil Engineering, University of Gonabad, Gonabad, 9691957678, Iran.*

Article Info
Received 03 April 2025
Accepted 13 July 2025
Available online 19 September 2025

Keywords:
Three-Dimensional Thermo-Elasticity;
Natural Frequency;
Functionally Graded Plate;
Elastic Foundation.

Abstract:
This research focuses on the analysis of free vibration of a rectangular plate made of multi-directional functionally graded materials on an elastic foundation, taking into account the effect of temperature. The temperature at different points of the plate may differ from its initial temperature, leading to the development of initial stresses within the plate. In this research, gradual variations in the mechanical properties of the material are possible in all three coordinate directions. Additionally, the mechanical properties of the material, except for the thermal conductivity coefficient, can be temperature-dependent. The governing equations are derived based on three-dimensional elasticity theory and discretized using the Generalized Differential Quadrature Method (GDQM). The validation of the proposed method demonstrates the high accuracy of the employed approach. Subsequently, several cases are solved, considering the effects of variations in the mechanical properties of the material in each coordinate direction or a combination of different directions, and the results are compared. The effects of temperature, elastic foundation stiffness, aspect ratio, thickness, power-law indices, and boundary conditions are investigated. The results indicate that an increase in temperature leads to a reduction in the vibrational frequency. Furthermore, the effect of temperature on frequency reduction is less pronounced for softer plates. In the case of one-directional property distribution, the frequency decreases with an increase in the power-law index. For multi-directional property distribution, the frequency initially decreases with an increase in the power-law index and then remains relatively unchanged.

***Corresponding Author:** mahdi.adineh@gonabad.ac.ir

Supplementary information: Supplementary information for this article is available at https://cste.journals.umz.ac.ir/

Please cite this paper as: Adineh, M., & Estiri, H. (2025). Effect of temperature on the natural frequency of multi-directional functionally graded rectangular plates on an elastic foundation using three-dimensional elasticity theory. Contributions of Science and Technology for Engineering, 2(4), 13-27. doi:10.22080/cste.2025.28914.1026.

1. Introduction

Frequency analysis of structures, particularly plates, has long been a subject of interest for researchers. Due to their relatively small thickness compared to the other two dimensions, plates are highly sensitive to vibrations. Xing et al. [1] derived a closed-form analytical solution for the free vibrations of functionally graded rectangular plates in a thermal environment. Kang et al. [2] studied the free vibrations of functionally graded rectangular plates in a thermal environment using three-dimensional elasticity theory. The effect of multiple hole distributions in functionally graded plates was investigated by Slimane et al. [3]. In this research, a high-order deformation theory has been employed to investigate the vibrational behavior of structures, including porosity distribution, which has been the focus of researchers. The influence of the porosity coefficient on the vibrational frequencies of the plate for various thickness ratios, geometric proportions, and different material properties has been among the achievements of this study. Hashemi and Jafari analyzed the nonlinear free vibration of functionally graded material plates with exponential distribution. They utilized the first-order shear deformation theory [4]. Kumar et al. [5] investigated the vibrational parameters of porous functionally graded plates, considering a foundation with variable thickness. In this study, higher-order shear deformation theories and various boundary conditions were employed. Kumar and Harsha studied the static and dynamic behavior of exponentially distributed functionally graded piezoelectric materials under thermo-electro-mechanical loading. They derived the governing equations using the first-order shear deformation theory and Hamilton's principle [6]. Shahverdi et al. proposed a method

*ISSN **3060-6578***

for solving the free vibration of arbitrarily shaped plates using the Generalized Differential Quadrature Method (GDQM) based on Kirchhoff's plate theory [7]. Hu and Fu examined the free vibration of porous plates using the first-order shear deformation theory. They applied four types of porosity distributions, each with three variations: power-law, exponential, and sigmoid distributions. These researchers investigated the effects of various factors, such as the width-to-thickness ratio, power-law index, porosity distribution, and ceramic materials. The results of this study revealed that in the exponential distribution, the frequency of non-uniform porosity increased significantly by approximately 67.3% compared to uniform porosity. In the case of uniform porosity, the frequency values for the sigmoid distribution increased by approximately 54% and 70%, respectively, compared to the power-law and exponential distributions [8].

Functionally graded materials have attracted significant attention in recent decades [9]. Although the earliest productions of such plates were probably one-dimensional, many applications in industries such as the energy industry (e.g., turbine blades exposed to very high temperatures and requiring resistance to applied stresses) demand surfaces with greater heat resistance, which necessitates the distribution of material phases in all three directions. Specifically, the higher the temperature that these components can withstand, the greater the efficiency and production of the device. On the other hand, this means reduced energy consumption and can lead to a decrease in environmental pollution. Moreover, nature, as a suitable model for advanced engineering designs, usually includes structures that are closer to functionally graded materials rather than completely isotropic materials. In nature, material distribution typically occurs in each coordinate direction as needed. It is not limited to a single direction (such as human bones, trees, etc.), which can serve as an appropriate pattern for developing engineering designs. Additionally, there may be a need to alter the natural frequencies of a designed structure when the geometry and boundary conditions cannot be significantly changed due to constraints, and the constituent materials have been specifically selected. In such cases, changes in the material distribution may be able to alter the natural frequency without causing any changes in geometry or boundary conditions. Investigating the numerical methods required for such analyses in structures, such as plates, and examining how the natural frequency changes with variations in material distribution can be helpful in various industries.

Multidirectionally functionally graded plates have gained significant attention in recent years. In addition to various analyses of these plates, such as bending and dynamic response [10-15], vibrations have also been investigated. Tahouneh and Naei [16] studied the vibrations of a rectangular plate made of bidirectional functionally graded materials under specific boundary conditions. In their study, material variations were allowed along the thickness and one in-plane direction. Still, due to the limitations of the solution method, variations in two in-plane directions were not feasible. Khorshidi et al. [17] studied the effect of a thermal environment on the free vibrations of bi-directional functionally graded rectangular plates on an elastic foundation using third-order shear deformation plate theory. Yin et al. [18] analyzed the free vibrations and buckling of in-plane functionally graded plates using higher-order shear deformation theory and the Iso-geometric method. Thai et al. [19] examined the bending and free vibrations of three-dimensional multi-directional functionally graded rectangular plates in a thermal environment using the Iso-geometric method. Xiang et al. [20] provided a three-dimensional solution for the free vibrations and buckling of rectangular plates with gradual material property variations in two in-plane directions. Adineh [21] studied the natural frequencies of multi-directional functionally graded rectangular plates on an elastic foundation using three-dimensional elasticity theory and the generalized differential quadrature method, without considering temperature effects. Ahlawat and Lal [22] investigated axisymmetric vibrations of multi-directional functionally graded circular plates under uniform in-plane loads resting on elastic foundations. The generalized differential quadrature method is applied to derive frequency equations from the governing differential equations for supported plates. Lahdiri and Kadsi [23] investigated the free vibration frequencies of imperfect tri-directional functionally graded material plates. The analysis covers multiple plate geometries with two porosity types (even and uneven) and different material configurations. Pham et al. [24] developed an analytical method to analyze the thermal vibration of multi-directional functionally graded porous (MFG) rectangular plates in fluid media. The mechanical properties of MFG porous plates vary along their length, width, and thickness directions. They used Hamilton's principle and refined the higher-order shear deformation plate theory.

Based on the reviewed literature, it can be concluded that a three-dimensional analysis of the free vibration of rectangular plates resting on an elastic foundation, considering the effects of temperature, has not yet been investigated. In the present study, the properties of materials, except for the thermal conductivity coefficient, are considered to be temperature dependent. In order to include the effect of temperature, a plate bending solution is performed under temperature conditions, and the stresses created as a result are calculated as residual stresses. Then, the calculated residual stresses are applied to the matrices, and an eigenvalue solution is performed to estimate the natural frequencies.

Both bending analysis and natural frequency determination of the plate have been investigated using the three-dimensional generalized differential quadrature method. This solution method allows for material variations to be considered in all coordinate directions and for the boundary conditions of each edge to be defined independently. A comparison of the obtained results with those available in published articles shows good agreement. The effects of various parameters, including material distribution exponents, plate thickness, length-to-width ratio, and temperature variations, on free vibrations have been investigated. Since three-dimensional elasticity theory was

used in this study, the obtained results can also serve as a reliable reference for validating future work.

2. Problem Definition

Figure 1 shows a multi-directional functionally graded rectangular plate resting on an elastic foundation. The origin of the coordinate system is assumed to be at the lower corner of the plate. The parameters a, b, and h represent the length of the plate in the x-direction, the length of the plate in the y-direction, and the thickness of the plate, respectively.

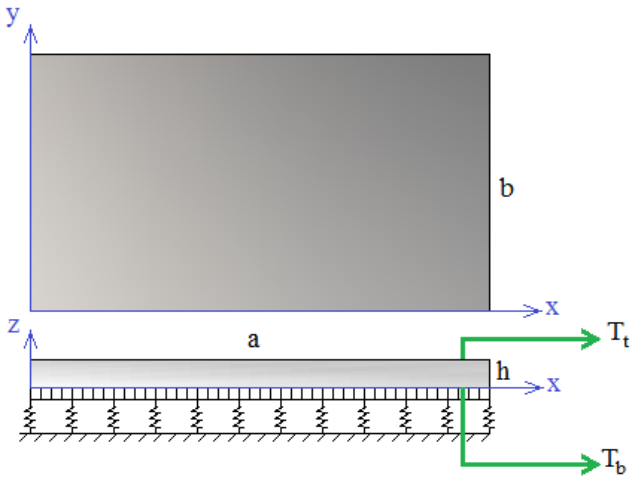

Figure 1. Multi-directional functionally graded rectangular plate resting on an elastic foundation under thermal loading

2.1. Material Distribution

In this research, gradual material variations exist in all three coordinate directions. Functionally graded plates are typically composed of two phases, where the material properties at different points of the plate gradually transition between the properties of these two phases according to specific relationships. These relationships can be power-law, exponential, or sigmoid. In most cases, one phase is a soft metal, and the other is a brittle and resistant material, such as ceramic. To determine the mechanical properties of the functionally graded plate, the linear rule of mixture is applied. Equation 1 represents this rule.

$$P = (P_1 - P_2)\left(\frac{x}{a}\right)^{n_x}\left(\frac{y}{b}\right)^{n_y}\left(\frac{z}{h}\right)^{n_z} + P_2 \quad (1)$$

Here, P represents the effective material property, such as the modulus of elasticity, Poisson's ratio, mass density, etc., at any point on the plate. In this article, the material distribution follows a power-law function. In this equation, n_x, n_y, and n_z are referred to as the power-law indices of the material distribution. To calculate the mechanical properties of the constituent material at any point on the plate, Equation 1 is used.

Additionally, all material properties except the thermal conductivity coefficient can be temperature-dependent. Equation 2 illustrates the nature of this dependency.

$$P = P_0(P_{-1}T^{-1} + 1 + P_1T + P_2T^2 + P_3T^3) \quad (2)$$

where P is a material property such as the elastic modulus, Poisson's ratio, or density; the P_i are constant coefficients determined based on the material type, and T is the temperature.

3. Formulation

3.1. Thermo-elastic Equations and Boundary Conditions

First, the initial stresses generated in the plate are calculated. For this purpose, a static thermo-elastic analysis is employed. The output of this analysis is the thermal stresses at all nodal points. Then, using the equations of motion, the stiffness and inertia matrices are extracted. Subsequently, the matrix equations required for solving the eigenvalue problem are formulated. Finally, by solving this system of equations, the natural frequency of vibration of the plate is obtained. The differential equation of heat transfer is represented by Equation 3. This equation is used to determine the temperature distribution within the plate.

$$-\frac{\partial}{\partial z}\left[K\frac{\partial T}{\partial z}\right] = 0 \quad (3)$$

In this Equation, K represents the thermal conductivity coefficient. This parameter can vary at different points on the plate. The boundary conditions applied are constant temperatures on the top and bottom surfaces of the plate. Equation 4 shows it.

$$T = T_t \text{ at } z=h \quad (4)$$

$$T = T_b \text{ at } z=0$$

The temperature distribution resulting from solving Equation 3 with the boundary conditions given by relations in Equation 4 for a plate made of isotropic materials or plates, in which material properties vary in the in-plane directions, is approximately a linear distribution through the thickness. However, for plates in which the thermal conductivity coefficient (K) varies through the thickness (such as one-directional functionally graded materials along the thickness or three-directional functionally graded materials), the temperature distribution deviates somewhat from the linear distribution.

Based on the fundamentals of elasticity theory, the equilibrium equations in three-dimensional space are given by Equations 5 to 7.

$$\frac{\partial \sigma_x}{\partial x} + \frac{\partial \tau_{xy}}{\partial y} + \frac{\partial \tau_{xz}}{\partial z} = 0 \quad (5)$$

$$\frac{\partial \tau_{xy}}{\partial x} + \frac{\partial \sigma_y}{\partial y} + \frac{\partial \tau_{yz}}{\partial z} = 0 \quad (6)$$

$$\frac{\partial \tau_{xz}}{\partial x} + \frac{\partial \tau_{yz}}{\partial y} + \frac{\partial \sigma_z}{\partial z} = 0 \quad (7)$$

The components of stress and strain (mechanical and thermal) are also related to each other by Equations 8 to 11.

$$\sigma_x = \frac{E}{(1+\nu)(1-\nu)}\left[(1-\nu)\varepsilon_x + \nu(\varepsilon_y + \varepsilon_z)\right] - \frac{E}{1-2\nu}\alpha(T - T_0) \quad (8)$$

$$\sigma_y = \frac{E}{(1+\nu)(1-\nu)}\left[(1-\nu)\varepsilon_y + \nu(\varepsilon_x + \varepsilon_z)\right] - \frac{E}{1-2\nu}\alpha(T-T_0) \quad (9)$$

$$\sigma_z = \frac{E}{(1+\nu)(1-\nu)}\left[(1-\nu)\varepsilon_z + \nu(\varepsilon_x + \varepsilon_y)\right] - \frac{E}{1-2\nu}\alpha(T-T_0) \quad (10)$$

$$\tau_{xy} = \frac{E}{(1+\nu)}\varepsilon_{xy}, \tau_{xz} = \frac{E}{(1+\nu)}\varepsilon_{xz}, \tau_{yz} = \frac{E}{(1+\nu)}\varepsilon_{yz} \quad (11)$$

Here, T_0 is the initial temperature of the plate. This value represents the temperature of the plate in a stress-free state. An increase in temperature relative to T_0 can lead to the development of initial stresses within the plate. Equations 12 and 13 represent the strain-displacement relationships.

$$\varepsilon_x = \frac{\partial u}{\partial x}, \varepsilon_y = \frac{\partial v}{\partial y}, \varepsilon_z = \frac{\partial w}{\partial z} \quad (12)$$

$$\varepsilon_{xy} = \frac{1}{2}\left(\frac{\partial u}{\partial y} + \frac{\partial v}{\partial x}\right), \varepsilon_{xz} = \frac{1}{2}\left(\frac{\partial u}{\partial z} + \frac{\partial w}{\partial x}\right), \varepsilon_{yz} = \frac{1}{2}\left(\frac{\partial v}{\partial z} + \frac{\partial w}{\partial y}\right) \quad (13)$$

In this research, four distinct boundary conditions are applied. The values of displacement and stress at these boundaries are defined according to Equations 14 to 17.

SSSS $$\begin{cases} x = 0, a \rightarrow v = w = \sigma_x = 0 \\ y = 0, b \rightarrow u = w = \sigma_y = 0 \end{cases} \quad (14)$$

SCSC $$\begin{cases} x = 0, a \rightarrow v = w = \sigma_x = 0 \\ y = 0, b \rightarrow u = v = w = 0 \end{cases} \quad (15)$$

CFCF $$\begin{cases} x = 0, a \rightarrow u = v = w = 0 \\ y = 0, b \rightarrow \sigma_y = \tau_{xy} = \tau_{yz} = 0 \end{cases} \quad (16)$$

CCCC $$\begin{cases} x = 0, a \rightarrow u = v = w = 0 \\ y = 0, b \rightarrow u = v = w = 0 \end{cases} \quad (17)$$

Additionally, the force boundary conditions on the top and bottom surfaces of the plate are considered, as outlined in Equations 18 and 19. Equation 18 states that no external force is applied to the top surface of the plate. Equation 19 represents the effect of the elastic foundation [16].

$$\sigma_z = 0, \tau_{xz} = \tau_{yz} = 0 \; at \;\; z = h \quad (18)$$

$$\sigma_z = k_w w - k_{sx}\frac{\partial^2 w}{\partial x^2} - k_{sy}\frac{\partial^2 w}{\partial y^2}, \tau_{xz} = \tau_{yz} = 0 \; at \; z=0 \quad (19)$$

In Equation 19, the parameters of the elastic foundation are determined according to the following relationships.

$$K_w = \frac{k_w a^4}{D_m}, J_{sx} = \frac{k_{sx} a^2}{D_m}, J_{sy} = \frac{k_{sy} b^2}{D_m} \quad (20)$$

$$D_m = {E_m h^3}\Big/{\left(12(1-{\nu_m}^2)\right)}$$

In these relationships, K_{sx}, K_{sy}, and K_w are constant values that determine the stiffness of the elastic foundation as they increase or decrease. E_m and ν_m represent the elastic modulus and Poisson's ratio of the metal phase in the functionally graded material, respectively. K_w, J_{sx} and J_{sy} are constant coefficients.

Using Equations 3 to 20, the thermal stresses generated within the plate are calculated. The stresses σ_x^0 and σ_y^0 are determined for all nodal points. In the subsequent analysis, these values are used as initial stresses. Using these stresses, the following expression is obtained. This value is added to the stiffness matrix used for calculating the eigenvalues [25]:

$$\sigma^0{}_x \frac{\partial^2 w}{\partial x^2} + \sigma^0{}_y \frac{\partial^2 w}{\partial y^2} \quad (21)$$

Next, the matrices required for solving the eigenvalue problem are determined using the equations of motion. Equations 22 to 24 represent the dynamic equilibrium equations in Cartesian coordinates based on three-dimensional elasticity theory.

$$\frac{\partial \sigma_x}{\partial x} + \frac{\partial \tau_{xy}}{\partial y} + \frac{\partial \tau_{xz}}{\partial z} = \rho\frac{\partial^2 u}{\partial t^2} \quad (22)$$

$$\frac{\partial \tau_{xy}}{\partial x} + \frac{\partial \sigma_y}{\partial y} + \frac{\partial \tau_{yz}}{\partial z} = \rho\frac{\partial^2 v}{\partial t^2} \quad (23)$$

$$\frac{\partial \tau_{xz}}{\partial x} + \frac{\partial \tau_{yz}}{\partial y} + \frac{\partial \sigma_z}{\partial z} = \rho\frac{\partial^2 w}{\partial t^2} \quad (24)$$

By substituting Equations 12 and 13 into Equations 8 to 11 and then inserting them into Equations 22 to 24, the equations of motion can be derived in terms of the displacement components. Equations 25 to 27 represent these Equations.

$$\begin{aligned} &\left(\frac{\frac{\partial E}{\partial x}(1+\nu)(1-2\nu) - E\left(\frac{\partial \nu}{\partial x}(1-2\nu) - 2\frac{\partial \nu}{\partial x}\right.}{(1+\nu)^2(1-2\nu)^2}\right. \\ &\left.-\nu)\frac{\partial u}{\partial x} + \nu\left(\frac{\partial v}{\partial y} + \frac{\partial w}{\partial z}\right)\right] \\ &+\frac{E}{(1+\nu)(1-2\nu)}\begin{bmatrix} -\frac{\partial v}{\partial x}\frac{\partial u}{\partial x} + (1-\nu)\frac{\partial^2 u}{\partial x^2} \\ +\frac{\partial v}{\partial x}\left(\frac{\partial v}{\partial y} + \frac{\partial w}{\partial z}\right) \\ +\nu\left(\frac{\partial^2 v}{\partial x \partial y} + \frac{\partial^2 w}{\partial x \partial z}\right) \end{bmatrix} \\ &-\frac{\frac{\partial E}{\partial x}(1-2\nu) + 2E\frac{\partial \nu}{\partial x}}{(1-2\nu)^2}\int_{T_0}^{T_p}\alpha dT \\ &-\frac{E}{(1-2\nu)}\frac{\partial\left(\int_{T_0}^{T_p}\alpha dT\right)}{\partial x} \end{aligned} \quad (25)$$

$$
\begin{aligned}
&+\frac{1}{2}\frac{\frac{\partial E}{\partial y}(1+\nu)-E\frac{\partial \nu}{\partial y}}{(1+\nu)^2}\left(\frac{\partial u}{\partial y}+\frac{\partial v}{\partial x}\right)\\
&\quad+\frac{1}{2}\frac{E}{(1+\nu)}\left(\frac{\partial^2 u}{\partial y^2}\right.\\
&\quad\left.+\frac{\partial^2 v}{\partial x\partial y}\right)\\
&+\frac{1}{2}\frac{\frac{\partial E}{\partial z}(1+\nu)-E\frac{\partial \nu}{\partial z}}{(1+\nu)^2}\left(\frac{\partial w}{\partial x}+\frac{\partial u}{\partial z}\right)\\
&\quad+\frac{1}{2}\frac{E}{(1+\nu)}\left(\frac{\partial^2 w}{\partial x\partial z}+\frac{\partial^2 u}{\partial z^2}\right)\\
&\quad=\rho\frac{\partial^2 u}{\partial t^2}
\end{aligned}
$$

$$
\begin{aligned}
&\frac{1}{2}\frac{\frac{\partial E}{\partial x}(1+\nu)-E\frac{\partial \nu}{\partial x}}{(1+\nu)^2}\left(\frac{\partial u}{\partial y}+\frac{\partial v}{\partial x}\right)\\
&+\frac{1}{2}\frac{E}{(1+\nu)}\left(\frac{\partial^2 u}{\partial x\partial y}+\frac{\partial^2 v}{\partial x^2}\right)\\
&+\left(\frac{\frac{\partial E}{\partial y}(1+\nu)(1-2\nu)-E\left(\frac{\partial \nu}{\partial y}(1-2\nu)-2\frac{\partial}{\partial}\right.\right.}{(1+\nu)^2(1-2\nu)^2}\\
&\left.-\nu)\frac{\partial v}{\partial y}+\nu\left(\frac{\partial u}{\partial x}+\frac{\partial w}{\partial z}\right)\right]\\
&+\frac{E}{(1+\nu)(1-2\nu)}\begin{bmatrix}-\frac{\partial \nu}{\partial y}\frac{\partial v}{\partial y}+(1-\nu)\frac{\partial^2 v}{\partial y^2}+\\ \frac{\partial \nu}{\partial y}\left(\frac{\partial u}{\partial x}+\frac{\partial w}{\partial z}\right)+\\ \nu\left(\frac{\partial^2 u}{\partial x\partial y}+\frac{\partial^2 w}{\partial y\partial z}\right)\end{bmatrix}\\
&-\frac{\frac{\partial E}{\partial y}(1-2\nu)+2E\frac{\partial \nu}{\partial y}}{(1-2\nu)^2}\int_{T_0}^{T_p}\alpha dT\\
&\quad-\frac{E}{(1-2\nu)}\frac{\partial\left(\int_{T_0}^{T_p}\alpha dT\right)}{\partial y}\\
&+\frac{1}{2}\frac{\frac{\partial E}{\partial z}(1+\nu)-E\frac{\partial \nu}{\partial z}}{(1+\nu)^2}\left(\frac{\partial v}{\partial z}+\frac{\partial w}{\partial y}\right)\\
&\quad+\frac{1}{2}\frac{E}{(1+\nu)}\left(\frac{\partial^2 v}{\partial z^2}+\frac{\partial^2 w}{\partial y\partial z}\right)\\
&\quad=\rho\frac{\partial^2 v}{\partial t^2}
\end{aligned}
\tag{26}
$$

$$
\begin{aligned}
&\frac{1}{2}\frac{\frac{\partial E}{\partial x}(1+\nu)-E\frac{\partial \nu}{\partial x}}{(1+\nu)^2}\left(\frac{\partial u}{\partial z}+\frac{\partial w}{\partial x}\right)\\
&\quad+\frac{1}{2}\frac{E}{(1+\nu)}\left(\frac{\partial^2 u}{\partial x\partial z}\right.\\
&\quad\left.+\frac{\partial^2 w}{\partial x^2}\right)\\
&+\frac{1}{2}\frac{\frac{\partial E}{\partial y}(1+\nu)-E\frac{\partial \nu}{\partial y}}{(1+\nu)^2}\left(\frac{\partial v}{\partial z}+\frac{\partial w}{\partial y}\right)\\
&\quad+\frac{1}{2}\frac{E}{(1+\nu)}\left(\frac{\partial^2 v}{\partial y\partial z}\right.\\
&\quad\left.+\frac{\partial^2 w}{\partial y^2}\right)\\
&+\left(\frac{\frac{\partial E}{\partial z}(1+\nu)(1-2\nu)-E\left(\frac{\partial \nu}{\partial z}(1-2\nu)-2\frac{\partial \nu}{\partial z}(1+\nu)\right)}{(1+\nu)^2(1-2\nu)^2}\right)\left[(1-\right.\\
&\left.\nu)\frac{\partial w}{\partial z}+\nu\left(\frac{\partial u}{\partial x}+\frac{\partial v}{\partial y}\right)\right]\\
&+\frac{E}{(1+\nu)(1-2\nu)}\begin{bmatrix}-\frac{\partial v}{\partial z}\frac{\partial w}{\partial z}+(1-\nu)\frac{\partial^2 w}{\partial z^2}\\ +\frac{\partial v}{\partial z}\left(\frac{\partial u}{\partial x}+\frac{\partial v}{\partial y}\right)\\ +\nu\left(\frac{\partial^2 u}{\partial x\partial z}+\frac{\partial^2 v}{\partial y\partial z}\right)\end{bmatrix}\\
&-\frac{\frac{\partial E}{\partial z}(1-2\nu)+2E\frac{\partial \nu}{\partial z}}{(1-2\nu)^2}\int_{T_0}^{T_p}\alpha dT\\
&\quad-\frac{E}{(1-2\nu)}\frac{\partial\left(\int_{T_0}^{T_p}\alpha dT\right)}{\partial z}\\
&\quad=\rho\frac{\partial^2 w}{\partial t^2}
\end{aligned}
\tag{27}
$$

3.2. Differential Quadrature Method

To discretize the Equations described in the previous section, the differential quadrature method is employed. In the differential quadrature method, the derivatives of a function are related to the values of the function at all nodal points within the domain. In this approach, the domain of the parameter l is divided into N points. Equation 28 represents the m-th order derivative of the function f with respect to the parameter l.

$$
\begin{aligned}
&\left.\frac{d^m f(x)}{dl^m}\right|_{n=n_i}=\sum_{j=1}^{N} C_{ij}^{(m)} f(l_j),\ i=\\
&1,2,\ldots,N\left.\frac{d^m f(x)}{\mathrm{d}l^m}\right|_{n=n_i}=\sum_{j=1}^{N} C_{\mathrm{ij}}^{(m)} f(l_j),\ \mathrm{i}=1,2,\ldots,\mathrm{N}
\end{aligned}
\tag{28}
$$

The weighting coefficients are denoted by $C_{ij}^{(m)}$. This coefficient is calculated for the first-order derivative using Equation 29. For higher-order derivatives, matrix multiplication according to Equation 30 can be used.

$$
\begin{aligned}
&C_{ij}^{(1)}=\frac{\prod_{j=1,j\neq i}^{N}(l_i-l_j)}{(l_i-l_k)\prod_{j=1,j\neq k}^{N}(l_k-l_j)},\\
&i,j,k=1,2,\ldots.,N\\
&C_{ii}^{(1)}=-\sum_{j=1,j\neq i}^{N} C_{ij}^{(1)},\\
&i=1,2,\ldots,N
\end{aligned}
\tag{29}
$$

$$
C_{\mathrm{ij}}^{(m)}=C_{\mathrm{ik}}^{(1)}C_{\mathrm{kj}}^{(m-1)}C_{\mathrm{ij}}^{(m)}=C_{\mathrm{ik}}^{(1)}C_{\mathrm{kj}}^{(m-1)} \tag{30}
$$

Additionally, the Chebyshev polynomial is used to determine the coordinates of the points within the domain. Equation 31 represents this polynomial. The parameter L in this equation denotes the length of the domain.

$$
l_i=0.5L\left(1-\frac{\cos(i-1)\times\pi}{N-1}\right) \tag{31}
$$

In the differential quadrature method, since the derivative of a function at each point is approximated by a linear combination of the function values at all nodal points, the equations usually reach accurate solutions with a relatively small number of points.

3.3. Calculation of Natural Frequencies

After discretizing the equations of motion, the stiffness matrix $[K_e]$ corresponding to those equations can be calculated. At this stage, the matrix $[K_T]$ related to thermal stresses is added to the stiffness matrix [25]:

$$[K] = [K_T] + [K_e][K] = [K_T] + [K_e] \quad (32)$$

where:

$$[K_T] = \begin{bmatrix} 0 & 0 & 0 \\ 0 & 0 & 0 \\ 0 & 0 & [K^T]_w \end{bmatrix} [K_T] = \begin{bmatrix} 0 & 0 & 0 \\ 0 & 0 & 0 \\ 0 & 0 & [K^T]_w \end{bmatrix} \quad (33)$$

The term $[K^T]_w$ is an n×n matrix, where n is the number of nodal points. The matrix $[K^T]_w$ is derived from the discretized coefficients of Equation 21. After substituting the discretized forms of the boundary conditions (Equations 14 to 20) into the appropriate nodal points, the stiffness matrix is completed. To obtain the natural frequencies, the nodal points corresponding to the equations of motion (d) and those where the boundary conditions are defined (b) are separated. Consequently, the stiffness matrix is also divided into four distinct parts. Equations 34 and 35 illustrate these cases.

$$\left[[K_{db}][K_{dd}]\right]\begin{Bmatrix}\{b\}\\\{d\}\end{Bmatrix} - \omega^2\left[[M_{db}][M_{dd}]\right]\begin{Bmatrix}\{b\}\\\{d\}\end{Bmatrix} = \{0\} \quad (34)$$

$$[K_{bd}]\{d\} + [K_{bb}]\{b\} = \{0\} \quad (35)$$

Based on the above relationships, the stiffness and mass matrices required for calculating the natural frequencies can be determined using Equations 36 and 38. Finally, by solving the eigenvalue problem of Equation 38, the natural frequencies are computed.

$$K_{nf} = [K_{dd}] - [K_{db}][K_{bb}]^{-1}[K_{bd}] \quad (36)$$

$$M_{nf} = [M_{dd}] - [M_{db}][K_{bb}]^{-1}[K_{bd}] \quad (37)$$

$$\left([K_{nf}] - \omega^2[M_{nf}]\right)\{d\} = \{0\} \quad (38)$$

4. Validation

To validate the proposed formulation, the first eight vibrational frequencies of a square plate made of the functionally graded material SUS304/Si3N4 are compared with the results from references [25-27]. The mechanical properties of this plate follow a power-law distribution similar to Equation 39.

$$P(z,T) = (P_U - P_L)\left(\frac{2z+h}{2h}\right)^p + P_L \quad (39)$$

Here, P represents a material property, such as the modulus of elasticity. Additionally, P_U and P_L denote the values of that property at the top and bottom surfaces of the plate (z=h and z=0), respectively. For validation, the power-law index p is assumed to be 2. The bottom surface of the plate is made of stainless steel SUS304, and the top surface is composed of silicon nitride Si3N4. The mechanical properties of these two materials are listed in Table 1. Furthermore, the constant coefficients of Equation 2 for these materials are also included in this Table.

Table 1. Mechanical Properties of SUS304 and Si3N4 Materials (parameters used in Equation 2) [9]

Material	property	P_{-1}	P_0	P_1	P_2	P_3
Si_3N_4	E (Pa)	0	348.43×10^9	-3.070×10^{-4}	2.160×10^{-7}	-8.946×10^{-11}
	ν	0	0.24	0	0	0
	$\alpha(\frac{1}{K})$	0	5.8723×10^{-6}	9.095×10^{-4}	0	0
	$\rho(\frac{kg}{m^3})$	0	2370	0	0	0
	$K(\frac{W}{mK})$	0	9.19	0	0	0
SUS304	E (Pa)	0	201.04×10^9	3.079×10^{-4}	-6.534×10^{-7}	0
	ν	0	0.3262	-2.002×10^{-4}	3.797×10^{-7}	0
	$\alpha(\frac{1}{K})$	0	12.330×10^{-6}	8.086×10^{-4}	0	0
	$\rho(\frac{kg}{m^3})$	0	8166	0	0	0
	$K(\frac{W}{mK})$	0	12.04	0	0	0

The plate under study is square with sides a=b=0.2 m and the thickness ratio of a/h=10. This plate is analysed under two conditions. In the first case, all four edges are clamped. In the second case, the plate has supported boundary conditions on all edges. Equation (40) represents the dimensionless natural frequency of the plate.

$$\omega = \frac{\omega b^2}{\pi^2}\sqrt{\frac{I_0}{D_0}} \quad (40)$$

where **ω** refers to the calculated and ω refers to the non-dimensionalized natural frequency, $I_0 = \rho_m h$ and $D_0 = \frac{E_m h^3}{12(1-\nu_m{}^2)}$. Additionally, ρ_m, E_m, and ν_m have values corresponding to the SUS304 material at the reference temperature of 300 K. The values of the first eight frequencies of this plate with clamped boundary conditions are listed in Table 2. The first observation from this table is the good agreement with the results published in references [25-27]. In the studied plates, the lower surface of the plate is at a temperature of 300 K, and the temperature difference

between the upper and lower surfaces of the plate is indicated as ΔT.

Table 2. Convergence and Validation of Natural Frequencies of a CCCC Functionally Graded Square Plate, a=b=10h=0.2m

ΔT	Reference	ω_1	ω_2	ω_3	ω_4	ω_5	ω_6	ω_7	ω_8
0	Yang and Shen [26]	4.1062	7.8902	7.8902	11.1834	12.5881	13.7867	15.4530	16.0017
	Kim [27]	4.1165	7.9696	7.9696	11.2198	13.1060	13.2089	15.9471	15.9471
	Li et al. [25]	4.1658	7.9389	7.9389	11.1212	13.0973	13.2234	15.3627	15.3627
	7 × 7 × 7	4.1430	8.1119	8.1119	11.2683	13.5805	13.7470	15.4554	15.4554
	9 × 9 × 9	4.1222	7.8648	7.8648	11.0271	12.9786	13.1017	15.4399	15.4399
	11 × 11 × 11	4.1152	7.8546	7.8546	11.0150	12.9867	13.1114	15.4375	15.4375
	13 × 13 × 13	4.1127	7.8510	7.8510	11.0108	12.9789	13.1030	15.4362	15.4362
300	Yang and Shen [26]	3.6636	7.2544	7.2544	10.3924	11.7054	12.3175	14.4520	15.0019
	Kim [27]	3.6593	7.3098	7.3098	10.4021	12.1982	12.3052	14.9090	14.9090
	Li et al. [25]	3.7202	7.3010	7.3010	10.3348	12.2256	12.3563	14.8112	14.8112
	7 × 7 × 7	3.7030	7.5049	7.5049	10.5136	12.7863	12.9609	14.9130	14.9130
	9 × 9 × 9	3.6817	7.2355	7.2355	10.2520	12.1185	12.2462	14.7213	14.7213
	11 × 11 × 11	3.6758	7.2308	7.2308	10.2476	12.1402	12.2703	14.7401	14.7401
	13 × 13 × 13	3.6743	7.2249	7.2249	10.2393	12.1269	12.2563	14.7279	14.7279
500	Yang and Shen [26]	3.6717	7.2210	7.2210	10.2348	12.1185	12.2473	14.7204	14.7204
	Kim [27]	3.2357	6.6281	6.6281	9.5900	10.8285	11.4350	13.4412	13.9756
	Li et al. [25]	3.2147	6.6561	6.6561	9.5761	11.2708	11.3812	13.8346	13.8346
	7 × 7 × 7	3.2741	6.6509	6.6509	9.5192	11.3126	11.4468	13.7907	13.7907
	9 × 9 × 9	3.2780	6.9079	6.9079	9.7558	11.9833	12.1661	14.1653	14.1653
	11 × 11 × 11	3.2548	6.6124	6.6124	9.4691	11.2384	11.3698	13.7104	13.7104
	13 × 13 × 13	3.2465	6.6010	6.6010	9.4555	11.2478	11.3811	13.7176	13.7176

Table 3 presents the results of the studied plate for SSSS boundary conditions. The results are compared with those from reference by Kang et al. [2].

In Table 4, the fundamental natural frequency of a homogeneous, supported square plate (a=b=1) resting on an elastic foundation is investigated. The Young's.modulus, Poisson's ratio, and density of the plate material are E_m=380 MPa, ν_m=0.3, and ρ_m=3800$\frac{kg}{m^3}$, respectively. The dimensionless natural frequency is defined according to Equation 41. The results demonstrate good agreement with those reported by Zhou et al. [28] and Hosseini-Hashemi et al. [29], particularly by Zhou et al. [28], which employed three-dimensional elasticity theory.

$$D_m = E_m h^3/12(1-{\nu_m}^2)$$
$$\omega = \frac{\omega a^2}{\pi^2}\sqrt{\frac{h\rho_m}{D_m}} \quad (41)$$

5. Numerical Examples

In this research, a rectangular functionally graded plate, whose mechanical properties vary in all three coordinate directions, has been investigated. This plate is analyzed under two boundary conditions. In one case, all four edges of the plate are clamped (CCCC). For the other boundary condition, the plate is solved with supported edges. The constituent materials of the plate are Si3N4 and SUS304. The temperature-dependent mechanical properties of these materials are listed in Table 1. The material distribution follows a power-law distribution, as shown in Equation 1. The temperature dependency of the material properties is in accordance with Equation 2. The dimensionless coefficients of the elastic foundation are determined based on Equation 20, and the dimensionless frequency is calculated using Equation 41, where the subscript m indicates that the properties of the metal phase (SUS304), have been used in this Equation.

Table 3. Convergence and Validation of Natural Frequencies of a SSSS Functionally Graded Square Plate, a=b=10h=0.2m

ΔT	Reference	ω_1	ω_2	ω_3	ω_4	ω_5	ω_6	ω_7	ω_8
0	Kang et al. [2]	2.4003	5.7316	5.7316	8.1033	8.1033	8.8040	10.7305	10.7318
	7 × 7 × 7	2.4002	5.6998	5.6998	8.1035	8.1035	8.7657	10.4931	10.4931
	9 × 9 × 9	2.3996	5.7340	5.7340	8.1033	8.1033	8.8056	10.7685	10.7685
	11 × 11 × 11	2.3997	5.7305	5.7305	8.1033	8.1033	8.8014	10.7270	10.7270
	13 × 13 × 13	2.3997	5.7306	5.7306	8.1033	8.1033	8.8015	10.7297	10.7297

	Kang et al. [2]	1.8923	5.1159	5.1159	7.7323	7.7323	8.0706	9.9209	9.9222
	7 × 7 × 7	1.8442	5.0470	5.0470	7.7906	7.7906	8.0017	9.6732	9.6732
300	9 × 9 × 9	1.8435	5.0824	5.0824	7.7904	7.7904	8.0418	9.9312	9.9312
	11 × 11 × 11	1.8435	5.0789	5.0789	7.7904	7.7904	8.0376	9.8896	9.8896
	13 × 13 × 13	1.8435	5.0789	5.0789	7.7904	7.7904	8.0377	9.8924	9.8924
	Kang et al. [2]	0.7264	4.0256	4.0256	6.7796	7.0273	7.0273	8.4896	8.4908
	7 × 7 × 7	0.7747	4.0348	4.0348	6.7978	7.1741	7.1741	8.3610	8.3610
600	9 × 9 × 9	0.7724	4.0709	4.0709	6.8359	7.1731	7.1731	8.5886	8.5886
	11 × 11 × 11	0.7725	4.0672	4.0672	6.8319	7.1732	7.1732	8.5479	8.5479
	13 × 13 × 13	0.7725	4.0673	4.0673	6.8320	7.1732	7.1732	8.5506	8.5506

Table 4. Convergence and Validation of Natural Frequencies of a SSSS Homogeneous Square Plate on an Elastic Foundation

h/a	K_w	$J_{sx}=J_{sy}$	$N_x \times N_y \times N_z$			Zhou et al. [28]	Hosseini-Hashemi et al. [29]
			7x7x7	9x9x9	11x11x11		
0.2	10	10	2.2542	2.2539	2.2539	2.2539	2.2722
0.2	0	10	2.2337	2.2334	2.2334	2.2334	2.2505
0.2	100	10	2.4302	2.4300	2.4300	2.4300	2.459
0.01	100	0	2.2417	2.2413	2.2413	2.2413	2.2413
0.01	100	10	2.6554	2.655	2.6551	2.6551	2.6551

Figure 2 shows the variations of the first natural frequency of a square plate with supported edges against the dimensionless elastic foundation coefficient (a=0.2 m, b=0.2 m, h=0.02 m, $J_{sx}=J_{sy}=100$). In this figure, as well as in the subsequent figures in this paper, the expression inside the parentheses indicates the power exponents of the material distribution function in Equation (1), i.e., (n_x, n_y, n_z). For example, (0, 0, 1) represents a one-directional functionally graded plate with graded material properties in the thickness direction, and (1, 1, 1) represents a three-directional functionally graded plate. As a first result, it can be observed that an increase in temperature leads to a reduction in the first natural frequency of the plate in all cases. An increase in temperature softens the plate, causing it to oscillate at a higher frequency. Additionally, in all solved examples, an increase in the stiffness of the elastic foundation increases in frequency. However, the change in frequency relative to foundation stiffness is initially small, as indicated by the shallow slope of the graph at the beginning. As the foundation stiffness increases, the slope of the graph also increases. In other words, the effect of foundation stiffness on the vibrational response of the plate becomes more pronounced. For very high values of elastic foundation stiffness, the graph approaches a horizontal line. This indicates that for tremendous values of elastic foundation stiffness, the first natural frequency becomes independent of the foundation stiffness.

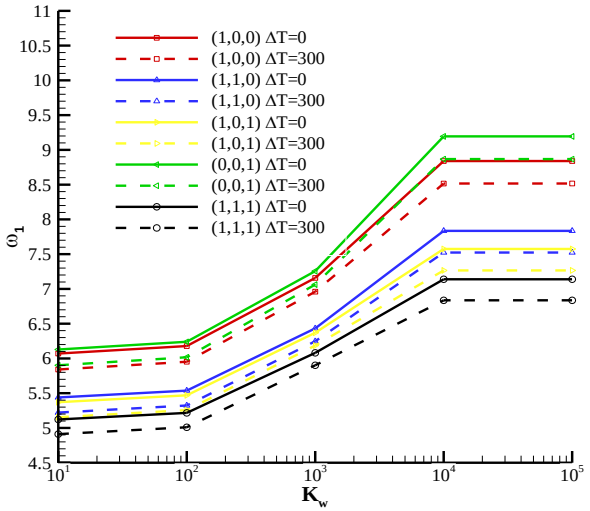

Figure 2. Variation of the first natural frequency of an SSSS FG plate on an elastic foundation versus Kw

The graphs in Figure 2 also reveal that the difference in the first natural frequency of the plate, with and without temperature effects, is more or less the same across all graphs for high foundation stiffness.

The previous plate is now analysed with clamped edges. Figure 3 shows the results of this analysis for the first natural frequency. The trend of the response is similar to that of the SSSS plate. However, the difference in frequency between the cases with and without temperature effects is smaller compared to the supported plate. For the CCCC plate, the first natural frequency converges to a constant value at very high stiffness values (greater than 10^6). In contrast, for the SSSS plate, the first natural frequency converges at stiffness values greater than 10^5. For stiffness values between 10^2 and 10^4, the slope of the graph for the clamped plate is steeper than that of the SSSS plate. In other words, the rate of change in the first natural frequency of the CCCC plate is higher than that of the supported plate for stiffness values between 10^2 and 10^4. In Figures 2 and 3, it is observed that the difference in the first natural frequency between the plate affected by temperature and the plate unaffected by temperature varies depending on the slope of the graph. Areas characterized by steeper slopes exhibit more minor variations in natural frequencies, while regions with gentler slopes show greater differences in these frequencies. This means that at lower and higher values of K_w, where the slope of the graph is minimal, the difference between the solid and dashed curves is more pronounced. Conversely, at intermediate values of K_w, where the slope increases, the difference between the two curves diminishes. This characteristic is more evident in Figure 3. This pattern is observed for all the different material distributions studied in Figures 2 and 3.

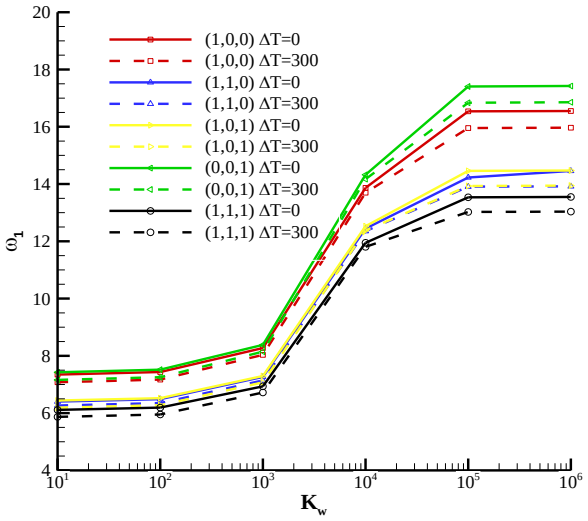

Figure 3. Variation of the first natural frequency of a CCCC FG plate on an elastic foundation versus Kw

In Figures 4 and 5, the effect of the length-to-width ratio a/b of the plate is investigated for SSSS and CCCC boundary conditions, respectively. The width of the plate in all calculations is b=0.04 m, and its length (a) varies between 0.04 m and 0.2 m (h=0.02 m, $K_w=J_{sx}=J_{sy}=100$). These graphs also indicate that an increase in temperature leads to a reduction in frequency. Heat softens the plate, resulting in a decrease in stiffness, which causes the plate to oscillate at a lower frequency. These figures show that although the material distribution has a significant effect on the first natural frequency of the plate, the difference between the temperature-affected and non-temperature-affected plates (solid and dashed graphs) follows a similar pattern across all material distributions. This trend holds for both types of boundary conditions. As the length-to-width ratio of the plate increases, the difference between the first natural frequency of the temperature-affected plate and the non-temperature-affected plate increases.

Figures 6 and 7 show the effect of thickness variation on the first natural frequency of a square plate for SSSS and CCCC boundary conditions, respectively. In these graphs, the elastic foundation coefficients are $K_w=J_{sx}=J_{sy}=100$ and a=b=0.2 m. These graphs indicate that an increase in thickness leads to a reduction in frequency. Increasing thickness enhances stiffness, which increases in frequency. However, if the thickness increases, the mass of the plate also increases, leading to a reduction in frequency. Therefore, it can be concluded that for the studied plates, the effect of increasing mass outweighs the effect of increasing stiffness, resulting in a decrease in frequency. Nevertheless, for the SSSS plate, as the thickness increases, the reduction in response becomes less pronounced. For the three-directional distribution of this plate, a 33% reduction in the dimensionless first natural frequency is observed when the thickness ratio increases from 0.1 to 0.2, 30% from 0.2 to 0.3, 25% from 0.3 to 0.4, and 21% from 0.4 to 0.5. In contrast, for the CCCC plate, a similar trend is not observed. The corresponding reductions for this plate are 12%, 17%, 24%, and 21%, respectively. Furthermore, an increase in temperature leads to a decrease in frequency. However, for thicker plates, this reduction is less pronounced, as indicated by the slope of the graphs.

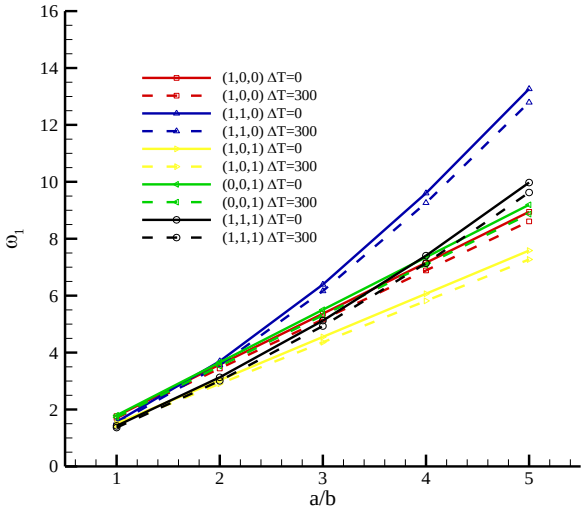

Figure 4. Variation of the first natural frequency of a SSSS FG plate on an elastic foundation versus the length-to-width ratio of the plate

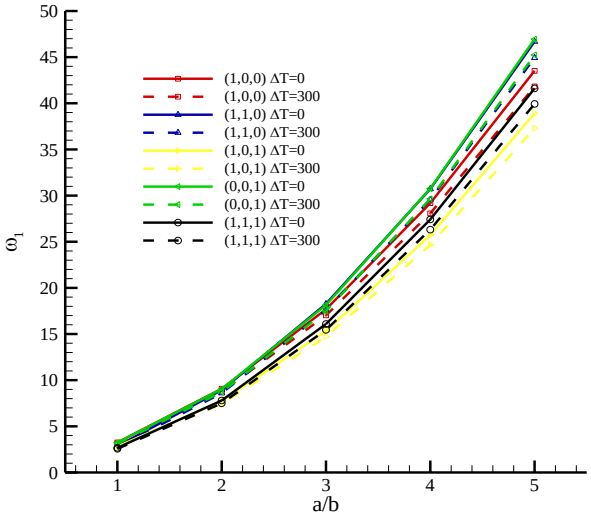

Figure 5. Variation of the first natural frequency of a CCCC FG plate on an elastic foundation versus the length-to-width ratio of the plate

In Figures 8 and 9, the effect of increasing the power-law index n of the material distribution function on the first natural frequency of the plate is shown (a=b=10h=0.2 m, Kw=Jsx=Jsy=100). Accordingly, with an increase in temperature, the slope of the graphs remains constant despite variations in n. In other words, the reduction in frequency in both cases (with and without temperature effects) is the same for different values of the power-law index n and for each distribution. These graphs show that as n increases in the case of one-directional distribution, the frequency decreases. However, the reduction is less pronounced for higher values of the power-law index. For example, when the power-law index increases from 1 to 5 for thickness-wise distribution, the frequency decreases by 14.8%, and when it increases from 5 to 10, the frequency decreases by 4.1% for the SSSS plate. For the CCCC plate, these values are 16% and 3.8%, respectively. In contrast, for multi-directional material property distribution, the frequency initially decreases significantly with an increase in the power-law index n and then remains relatively unchanged. The slope of the graphs indicates this. Thickness-wise one-directional distribution results in a higher frequency compared to in-plane one-directional distribution, as previously observed. However, for two-directional distribution, if the distribution is along the length and width, the frequency is higher than for a two-directional distribution where one direction is the thickness, although the difference is not significant. This trend is slightly different for the CCCC plate, as can be seen in Figure 9 for linear material distribution (n=1).

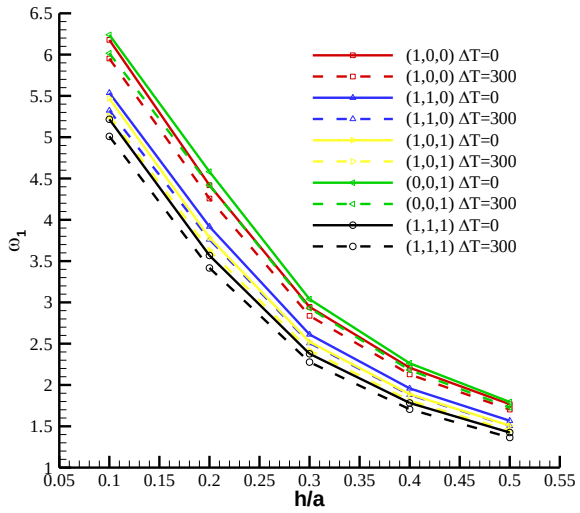

Figure 6. Variation of the first natural frequency of an SSSS FG plate on an elastic foundation versus thickness

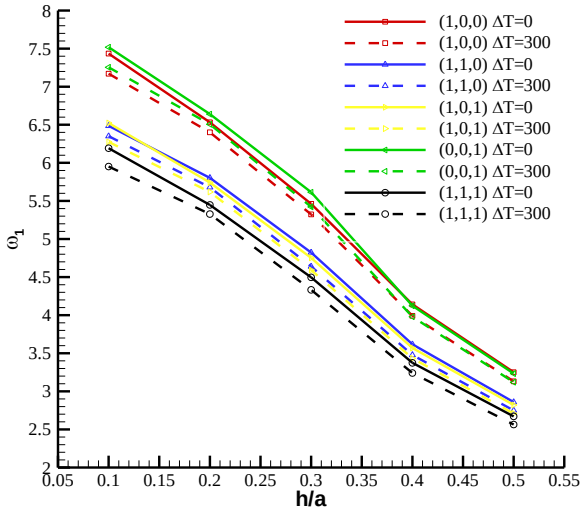

Figure 7. Variation of the first natural frequency of a CCCC FG plate on an elastic foundation versus thickness

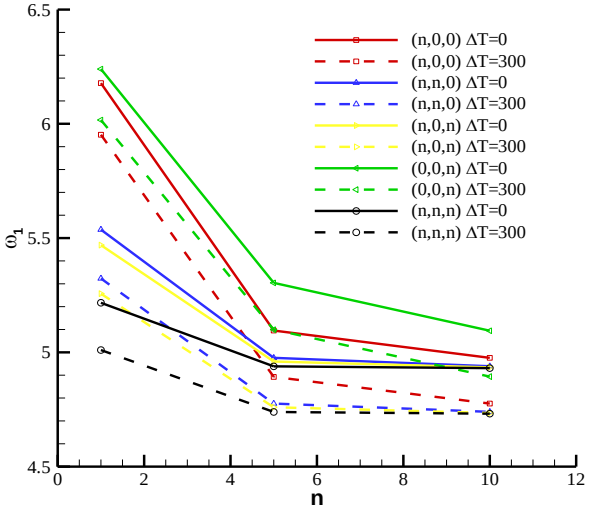

Figure 8. Variation of the first natural frequency of an SSSS FG plate on an elastic foundation versus power-law index

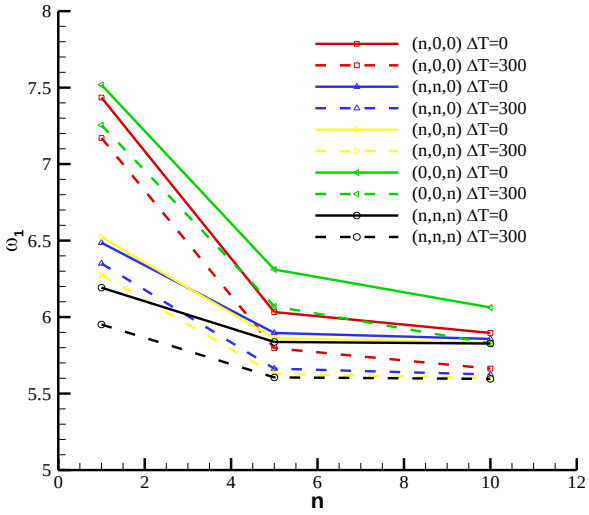

Figure 9. Variation of the first natural frequency of a CCCC FG plate on an elastic foundation versus power-law index

In Figure 10, the effect of boundary conditions on the first natural frequency of the plate is investigated ($a=b=10h=0.2$ m, $K_w=J_{sx}=J_{sy}=100$). Based on these graphs, the stiffer the boundary conditions, the higher the frequency of the plate. The CCCC plate, with all four edges clamped, exhibits the highest frequency. In contrast, the FCFC plate, with two free edges, has the lowest frequency. Between these two plates, the SSSS and SCSC plates are positioned, with two and four supported edges, respectively, which are softer compared to clamped edges. Figure 10 shows that the effect of temperature in reducing the frequency is less pronounced for softer plates. Therefore, the difference in frequency between the cases with and without temperature effects is less for the FCFC plate compared to the CCCC plate. Additionally, the direction of material distribution has a significant impact on the response for one-directional distribution in the FCFC plate. Specifically, the dimensionless frequency for thickness-wise one-directional distribution is 4.9, while for in-plane one-directional distribution, it is 4.05, indicating a difference of approximately 20%. In contrast, for other plates and material distribution types, such a difference is not observed.

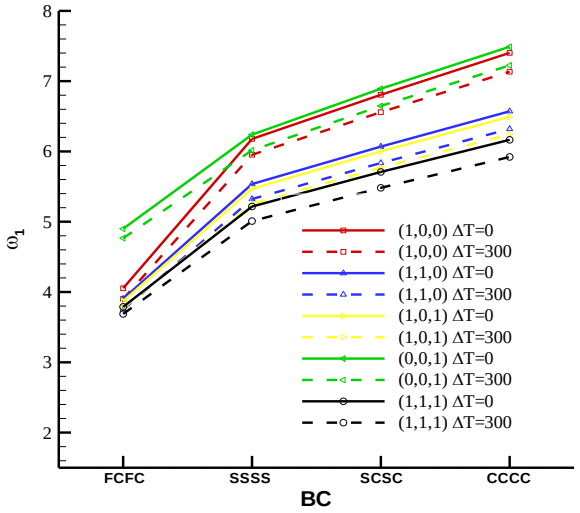

Figure 10. Variation of the first natural frequency of an FG plate on an elastic foundation versus different boundary conditions

Finally, the effect of increasing temperature on the first natural frequency is investigated (a=b=10h=0.2 m, Kw=Jsx=Jsy=100). Figures 11 and 12 show the responses for the SSSS and CCCC plates, respectively. These graphs indicate that an increase in temperature leads to a reduction in the vibrational frequency. This can be explained by the fact that an increase in temperature softens the plate, resulting in a decrease in stiffness. Consequently, the frequency also decreases. It should be noted that as the temperature increases further, the reduction in frequency becomes less pronounced. The slopes of the graphs illustrate this point. Based on Figures 11 and 12, the difference in frequency due to the direction of material distribution at various temperatures was found to be consistent. In other

words, the slopes of the graphs for one-directional distribution are equal. This consistency in slope also applies to two-directional distribution. However, a slight difference was observed for the CCCC plate with a two-directional distribution.

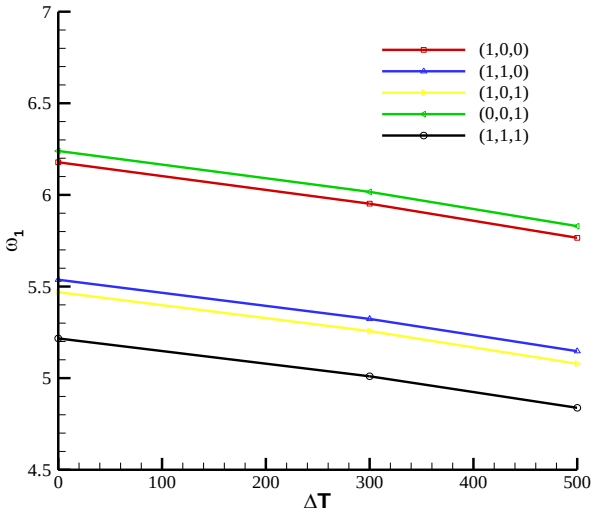

Figure 11. Variation of the first natural frequency of an SSSS FG plate on an elastic foundation versus ΔT

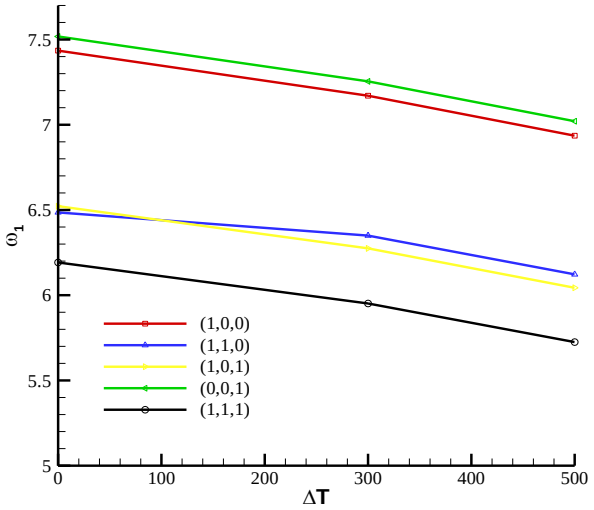

Figure 12. Variation of the first natural frequency of a CCCC FG plate on an elastic foundation versus ΔT

6. Conclusions

In this research, for the first time, the natural frequencies of a multi-directional functionally graded rectangular plate on an elastic foundation in a thermal environment were studied using three-dimensional elasticity theory. A power-law distribution function was used to determine the distribution of mechanical properties at different points on the plate. The generalized differential quadrature method was employed to discretize the equations. All mechanical properties related to the free vibrations of the plate, including Poisson's ratio, were considered with the possibility of variation in all three coordinate directions. Additionally, all material properties, except for the thermal conductivity coefficient, were temperature-dependent. Various factors, such as the direction of material variation, the effect of elastic foundation parameters, boundary conditions, geometric aspect ratios of the plate, and plate temperature, were investigated. The results showed that although the direction of material variation (thickness-wise, in-plane, or various combinations thereof) can have a significant impact on the natural frequency of the plate, the effect of plate temperature on its first natural frequency does not depend much on the direction of material distribution. The results showed that for very high and very low elastic foundation coefficient (K_w). In those regions, the first natural frequency depends less on the change in the K_w coefficient, the difference between the plate under the influence of temperature and the plate without the influence of temperature is greater, and in regions where the values of the first natural frequency are more sensitive to the K_w, the difference between the two is smaller. From the graphs shown, it can be seen that as the length to width ratio of the

plate increases, the difference in the magnitude of the first natural frequency of the plate affected by temperature and the plate without temperature effects increases. The results also showed that with increasing plate thickness, the decrease in the first natural frequency due to temperature application decreases slightly. Another result of this study was the lesser effect of temperature in reducing the frequency of plates with softer boundary conditions. Additionally, as the temperature increased, the reduction in vibrational frequency became less pronounced.

7. References

[1] Xing, Y. F., Wang, Z. K., & Xu, T. F. (2018). Closed-form Analytical Solutions for Free Vibration of Rectangular Functionally Graded Thin Plates in Thermal Environment. International Journal of Applied Mechanics, 10(3). doi:10.1142/S1758825118500254.

[2] Kang, R., Xin, F., Shen, C., & Lu, T. J. (2022). 3D Free Vibration Analysis of Functionally Graded Plates with Arbitrary Boundary Conditions in Thermal Environment. Advanced Engineering Materials, 24(5). doi:10.1002/adem.202100636.

[3] Slimane, M., Adda, H. M., Mohamed, M., Hakima, B., Hadjira, H., & Sabrina, B. (2020). Effects of even pores distribution of functionally graded plate porous rectangular and square. Procedia Structural Integrity, 26, 35–45. doi:10.1016/j.prostr.2020.06.006.

[4] Hashemi, S., & Jafari, A. A. (2020). Nonlinear free vibration analysis of functionally graded rectangular plate using modified Lindstedt-Poincare method. Journal of Science and Technology of Composites, 6(4), 637-648. doi:10.22068/JSTC.2019.106866.1542.

[5] Kumar, V., Singh, S. J., Saran, V. H., & Harsha, S. P. (2021). Vibration characteristics of porous FGM plate with variable thickness resting on Pasternak's foundation. European Journal of Mechanics, A/Solids, 85. doi:10.1016/j.euromechsol.2020.104124.

[6] Kumar, P., & Harsha, S. P. (2021). Vibration response analysis of exponential functionally graded piezoelectric (EFGP) plate subjected to thermo-electro-mechanical load. Composite Structures, 267. doi:10.1016/j.compstruct.2021.113901.

[7] Shahverdi, H., Navardi, M. M., & Sadr, M. H. (2022). A Proposed Approach to Simulate Thin Quadrilateral Plates Using Generalized Differential Quadrature Method Based on Kirchhoff–Love Theory. AUT Journal of Mechanical Engineering, 6(1), 15–30. doi:10.22060/ajme.2021.20283.5995.

[8] Hu, X., & Fu, T. (2023). Free vibration analysis of functionally graded plates with different porosity distributions and grading patterns. Journal of Mechanical Science and Technology, 37(11), 5725–5738. doi:10.1007/s12206-023-1012-6.

[9] Adineh, M., & Kadkhodayan, M. (2017). Three-dimensional thermo-elastic analysis of multi-directional functionally graded rectangular plates on elastic foundation. Acta Mechanica, 228(3), 881–899. doi:10.1007/s00707-016-1743-x.

[10] Adineh, M., & Kadkhodayan, M. (2017). Three-dimensional thermo-elastic analysis and dynamic response of a multi-directional functionally graded skew plate on elastic foundation. Composites Part B: Engineering, 125, 227–240. doi:10.1016/j.compositesb.2017.05.070.

[11] Rajasekaran, S., Khaniki, H. B., & Ghayesh, M. H. (2022). Thermo-mechanics of multi-directional functionally graded elastic sandwich plates. Thin-Walled Structures, 176, 109266. doi:10.1016/j.tws.2022.109266.

[12] Tran, M. T., & Thai, S. (2023). Transient analysis of variable thickness multi-directional functionally graded plates using isogeometric analysis. Multidiscipline Modeling in Materials and Structures, 19(4), 652–679. doi:10.1108/MMMS-12-2022-0283.

[13] Kumar, S., & Kar, V. R. (2022). Three-dimensional thermal analysis of multidirectional (perfect/porous) functionally graded plate under in-plane heat flux. Materials Today: Proceedings, 56, 879–882. doi:10.1016/j.matpr.2022.02.524.

[14] Thai, S., Do, D. T. T., & Tan, T. N. (2022). Nonlinear bending analysis of variable thickness multi-directional functionally graded plates based on isogeometric analysis. Mechanics of Advanced Materials and Structures, 30(20), 4091–4109. doi:10.1080/15376494.2022.2088909.

[15] Srivastava, M. C., & Singh, J. (2023). Influences of elastic foundation on bending analysis of multidirectional porous functionally graded plate under industrial used loading: a meshfree approach. Multiscale and Multidisciplinary Modeling, Experiments and Design, 6(4), 519–535. doi:10.1007/s41939-023-00156-x.

[16] Tahouneh, V., & Naei, M. H. (2014). A novel 2-D six-parameter power-law distribution for three-dimensional dynamic analysis of thick multi-directional functionally graded rectangular plates resting on a two-parameter elastic foundation. Meccanica, 49(1), 91–109. doi:10.1007/s11012-013-9776-x.

[17] Khorshidi, K., Bakhsheshi, A., & Ghadirian, H. (2016). The study of the effects of thermal environment on free vibration analysis of two dimensional functionally graded rectangular plates on Pasternak elastic foundation. doi:10.22044/JSFM.2016.792

[18] Yin, S., Yu, T., Bui, T. Q., Zheng, X., & Tanaka, S. (2016). In-plane material inhomogeneity of functionally graded plates: A higher-order shear deformation plate isogeometric analysis. Composites Part B: Engineering, 106, 273–284. doi:10.1016/j.compositesb.2016.09.008.

[19] Thai, S., Nguyen, V. X., & Lieu, Q. X. (2022). Bending and free vibration analyses of multi-directional functionally graded plates in thermal environment: A three-dimensional Isogeometric Analysis approach. Composite Structures, 295. doi:10.1016/j.compstruct.2022.115797.

[20] Xiang, T., Natarajan, S., Mana, H., Song, C., & Gao, W. (2014). Free vibration and mechanical buckling of plates

with in-plane material inhomogeneity-A three dimensional consistent approach. Composite Structures, 118(1), 634–642. doi:10.1016/j.compstruct.2014.07.043.

[21] Adineh, M. (2024). Natural Frequency analysis of Multi-directional Functionally Graded Rectangular Plates on elastic Foundation using Three-dimensional Elasticity Theory. Mechanic of Advanced and Smart Materials, 4(1), 40–63. doi:10.61186/masm.4.1.40.

[22] Ahlawat, N., & Lal, R. (2016). Buckling and Vibrations of Multi-directional Functionally Graded Circular Plate Resting on Elastic Foundation. Procedia Engineering, 144, 85–93. doi:10.1016/j.proeng.2016.05.010.

[23] Lahdiri, A., & Kadri, M. (2022). Free vibration behaviour of multi-directional functionally graded imperfect plates using 3D isogeometric approach. Earthquake and Structures, 22(5), 527–538. doi:10.12989/eas.2022.22.5.527.

[24] Pham, Q. H., Tran, V. K., & Nguyen, P. C. (2024). Exact solution for thermal vibration of multi-directional functionally graded porous plates submerged in fluid medium. Defence Technology, 35, 77–99. doi:10.1016/j.dt.2023.09.004.

[25] Li, Q., Iu, V. P., & Kou, K. P. (2009). Three-dimensional vibration analysis of functionally graded material plates in thermal environment. Journal of Sound and Vibration, 324(3–5), 733–750. doi:10.1016/j.jsv.2009.02.036.

[26] Yang, J., & Shen, H. S. (2002). Vibration characteristics and transient response of shear-deformable functionally graded plates in thermal environments. Journal of Sound and Vibration, 255(3), 579–602. doi:10.1006/jsvi.2001.4161.

[27] Kim, Y. W. (2005). Temperature dependent vibration analysis of functionally graded rectangular plates. Journal of Sound and Vibration, 284(3–5), 531–549. doi:10.1016/j.jsv.2004.06.043.

[28] Zhou, D., Cheung, Y. K., Lo, S. H., & Au, F. T. K. (2004). Three-dimensional vibration analysis of rectangular thick plates on Pasternak foundation. International Journal for Numerical Methods in Engineering, 59(10), 1313–1334. doi:10.1002/nme.915.

[29] Hosseini-Hashemi, S., Rokni Damavandi Taher, H., Akhavan, H., & Omidi, M. (2010). Free vibration of functionally graded rectangular plates using first-order shear deformation plate theory. Applied Mathematical Modelling, 34(5), 1276–1291. doi:10.1016/j.apm.2009.08.008.